Astronomy
&
Astrophysics

The transition from soluble to insoluble organic matter in interstellar ice analogs and meteorites

Grégoire Danger[1,2,3], Alexander Ruf[1,4], Thomas Javelle[1], Julien Maillard[5], Vassilissa Vinogradoff[1,2], Carlos Afonso[5], Isabelle Schmitz-Afonso[5], Laurent Remusat[6], Zelimir Gabelica[7], and Philippe Schmitt-Kopplin[8,9]

[1] Aix-Marseille University, CNRS, Institut Origines, PIIM, Marseille, France
 e-mail: gregoire.danger@univ-amu.fr
[2] Aix Marseille Université, Laboratoire d'Astrophysique de Marseille, UMR 7326, CNRS, CNES, Marseille, France
[3] Institut Universitaire de France (IUF), Paris, France
[4] Ludwig-Maximilians-University, Department of Chemistry and Pharmacy, Butenandtstr. 5-13, 81377 Munich, Germany
 and Excellence Cluster ORIGINS, Boltzmannstraße 2, 85748 Garching, Germany
 e-mail: alexander.ruf@cup.uni-muenchen.de
[5] Normandie Univ., COBRA UMR 6014 et FR 3038 Univ. Rouen; INSA Rouen; CNRS IRCOF, 1 Rue Tesnière,
 76821 Mont-Saint-Aignan Cedex, France
[6] Muséum National d'Histoire Naturelle, Sorbonne Université, UMR CNRS 7590, Institut de minéralogie, de physique des matériaux
 et de cosmochimie, Paris, France
[7] Université de Haute-Alsace, ENSCMu, Lab. GSEC, 3 Rue Alfred Werner, 68093 Mulhouse Cedex, France
[8] Helmholtz Zentrum München, Analytical BioGeoChemistry, Neuherberg, Germany
[9] Technische Universität München, Chair of Analytical Food Chemistry, Freising-Weihenstephan, Germany

ABSTRACT

Context. Carbonaceous chondrites are sources of information on the origin of the Solar System. Their organic content is conventionally classified as soluble (SOM) and insoluble organic matter (IOM), where the latter represents the majority.
Aims. In this work, our objectives are to identify possible relations between soluble and insoluble organic matter generated in laboratory experiments and to extrapolate the laboratory analog findings to soluble and insoluble organic matter of meteorites to test their connection.
Methods. Using laboratory experiments, processes possibly linking IOM analog (IOMA) to SOM analog (SOMA) precursors are investigated by assuming that dense molecular ices are one of the sources of organic matter in the Solar System. Each organic fraction is analyzed by laser desorption coupled to a Fourier transform ion cyclotron resonance mass spectrometer on a comprehensive basis.
Results. SOMA and IOMA significantly differ in their chemical fingerprints, and particularly in their aromaticity, O/C, and N/C elemental ratios. Using an innovative molecular network, the SOMA–IOMA transition was tested, revealing connection between both classes. This new network suggests that IOMA is formed in two steps: a first generation IOMA based on precursors from SOMA, while a second IOMA generation is formed by altering the first IOMA generation. Finally, using the same analytical technique, the molecular content of IOMA and that of the Paris IOM are compared, showing their molecular similarities for the first time. The molecular network application to the Paris SOM and IOM demonstrates that a possible connection related to photochemical ice processing is present, but that the overall history of IOM formation in meteorites is much more complex and might have been affected by additional factors (e.g., aqueous alteration).
Conclusions. Our approach provides a new way to analyze the organic fraction of extraterrestrial material, giving new insights into the evolution of organic matter in the Solar System.

Key words. astrochemistry – astrobiology – molecular processes – methods: laboratory: molecular – methods: analytical –
meteorites, meteors, meteoroids

1. Introduction

Organic matter is diversely present in many astrophysical environments, from the interstellar medium to the interplanetary bodies and planets of the Solar System (Ruf et al. 2018). While observations give information on the organic composition of some astrophysical objects, the actual molecular diversity has only been observed on Earth for fragments of asteroids and comets (carbonaceous chondritic meteorites; Schmitt-Kopplin et al. 2010, 2012; Ruf et al. 2019b). Carbonaceous matter represents up to 6% of the weight of these meteorites (Pearson et al. 2006). Depending on extraction protocols, two fractions can be recovered. A soluble fraction, called soluble organic matter (SOM), which presents a high molecular diversity as identified

by high resolution mass spectrometry analyses (HRMS; Schmitt-Kopplin et al. 2010). Targeted analyses have identified numerous molecular families, ranging from amino acids, sugar derivatives, and nucleobases, to various polyaromatic hydrocarbon (PAH) compounds composing this SOM (Pizzarello 2007). Along with SOM, an insoluble organic fraction can be isolated after successive demineralization steps, and this is called insoluble organic matter (IOM). This IOM is generally seen as an agglomerate of hydrophobic macromolecules formed by small PAH units cross-linked with aliphatic bridges including a small amount of heteroatoms such as O, N, or S (Cody et al. 2002; Gardinier et al. 2000; Remusat et al. 2005a,b; Yabuta et al. 2005). This high molecular diversity was also observed when applying laser desorption ionization HRMS (LDI-HRMS)

to IOM, showing thousands of organic molecules with masses ranging from 150 to 700 unified atomic mass units (u), (Danger et al. 2020). These molecules are mainly formed by aromatic or condensed aromatic structures, including small amounts of heteroatoms (O, N, and/or S). A possible origin of this type of organic matters could be related to ices observed in dense molecular clouds of the interstellar medium (Danger et al. 2021). Their isotopic measurements showed an enrichment in heavier elements (^{13}C, ^{15}N and/or D), implying reactivity occurring at low temperatures (Remusat et al. 2010).

To complement spectral observations and meteorite analyses, experimental simulations were developed in the laboratory to verify different hypotheses and steps that could lead to the organic matter observed in meteorites. For this purpose, the evolution of dense molecular ices during a planetary system formation is simulated. These experiments show that ice irradiation by energetic particles (UV photons at Lyman α, electrons or ions) followed by thermal processes results in diverse molecular fingerprints comparable those of meteorites (Danger et al. 2016). However, significant differences remain, such as the nitrogen content, which is higher in analogs compared to meteorites. This maybe be a result of the alteration of meteoritic parent bodies, as observed in the mineralogy of carbonaceous meteorites (Brearley 2006; Vinogradoff et al. 2017). Particularly, for some objects, aqueous alteration is observed as predominant (Le Guillou et al. 2014; Le Guillou & Brearley 2014). We thus consider here that such an organic residue formed in the laboratory could be considered a pre-accretional organic analog (Danger et al. 2021). The UV irradiation at Lyman α of this pre-accetional organic analog, initially soluble in polar solvents, shows the formation of a crust at its surface, which turned out to be an insoluble fraction. Infrared spectroscopy analyses suggest some similarities with meteorite IOM (de Marcellus et al. 2017), but this technique lacked the molecular resolution, specificity, and sensitivity necessary to obtain unambiguous characterization and meteorite comparison.

In this work, experiments were performed to produce both soluble and insoluble organic matter analogs (SOMA and IOMA, respectively) and probe their transition. These samples were analyzed by laser desorption ionization using a Fourier transform resonance cyclotron mass spectrometer (LDI-FTICR-MS; Maillard et al. 2018). This technique has shown its ability to analyze a fraction of meteorite IOM (Danger et al. 2020) underlying the molecular diversity present in IOM. Using specific data representation, the SOMA/IOMA transition was investigated, showing a two-step process for the IOMA formation. Finally, IOMA and the IOM of Paris meteorite were compared, and the similarities observed may highlight that dense molecular ices have to be considered as an essential source of organics for the Solar System.

2. Experimental results and analysis

2.1. Soluble versus insoluble organic matter analogues (SOMA vs. IOMA)

The soluble analog was firstly produced at 77 K from an ice analog composed of H_2O, CH_3OH, and NH_3 in a ratio of 2:1:1 and concomitantly deposited and UV irradiated at Lyman α over 72h. The SOMA was directly analyzed by LDI-FTICR-MS in positive ionization mode. Figure 1A displays the mass spectrum from which 3756 molecular formulas were attributed. The CHNO group represents 88% of the attributions, whereas the CHN group represents the other 12%. CHO molecules are not

observed. The O atoms are widely distributed in a mass range between 150 and 800 u (Fig. B.1) ranging from 1 to 10 atoms per molecule, with a maximum of four O atoms per attribution (Fig. B.2). For N atoms, the distribution profile is different as two distributions are visible (Figs. 1B and B.1). One distribution from 200 to 800 u (Zone A) is more enriched in nitrogen (from 8 to 20 N), while another distribution from 150 to 800 u displays lower N counts from 2 to 14 (Zone B). As shown in Fig. B.1, these two distributions are absent for O. They are also visible in the evolution of N counts per molecular formula as two maxima are visible, one at N_6 and another at N_{17} (Fig. B.2). On average, attributions present higher N_8 than in O_3 contents. This is different to what was observed in electrospray ionization (ESI), since for the same ice, on average the number of N and O were equivalent (Danger et al. 2013, 2016; Fresneau et al. 2017). The average number of C is 19, with an H average of 28.

The two distributions that differ by the number of N are also identified by the represented double bond equivalent (DBE) versus the number of carbon plots (Figs. 1B and B.3). Zone A presents the highest DBE for a similar C count (Fig. 1B). Zone A is enriched in N and depleted in O, and it includes CHNO molecules and a large part of the CHN group (Fig. B.3). In contrast, Zone B is depleted in N and enriched in O, with a lower DBE. These two distributions can be related to the ones observed with ESI, where the nitrogen-enriched distribution detected in positive ESI mode can be related to Zone A, and the carbon-rich distribution can be related to Zone B (Fresneau et al. 2017).

The X_C pie charts (Fig. 1B), with $m = 0.5$ for SOMA and $m = 0.75$ for IOMA, confirm the higher aromaticity of Zone A, since 97% can be related to condensed aromatic structures, 2% to aromatics and only 0.2% to aliphatics. For Zone B, aliphatics represent 15%, while condensed aromatics decrease to 50%, and aromatics represent 35% of all molecular formulas. With LDI, the SOMA presents a higher aromaticity than observed in previous works with ESI, due to the different ionization selectivity between these two ionization techniques. LDI in positive mode tends to favor the ionization of unsaturated structures and molecules bearing nitrogen (Cho et al. 2013). This is also corroborated by van Krevelen (VK) representations that present lower H/C and N/C (Fig. 1C) compared to ESI mode, even if H/C is not lower to due to the high level of N in the molecular formula. However, similar distributions of compounds are observed in the VK space, implying similar distributions of compounds such as unsaturated hydrocarbons or aromatic structures with low amounts of O and various nitrogen chemical functions. For high DBE, we can assume that N is incorporated in the backbone of molecules, especially for molecules included in Zone A (Fresneau et al. 2017).

To evolve toward IOMA, the SOMA was further irradiated with UV. Only the first 0.1 µm of the SOMA were affected (de Marcellus et al. 2017). Therefore, a thin layer of IOMA is formed at the top of the SOMA (de Marcellus et al. 2017). The IOMA mass spectrum is different to SOMA (Fig. 1A). The number of attributions is 9738 for IOMA, three times more than for SOMA. The molecular structures of the IOMA are more easily ionized by LDI, indicating a potential higher aromaticity (Cho et al. 2013). This is supported by the DBE versus #C and X_C representations (Fig. 1B), where the detected compounds show PAH characteristics, and structures were mainly related to condensed aromatic ones (93%). This is also visible in the VK representation, which is very different from the SOMA one (Figs. 1C and B.4). In IOMA, attributions extend to H/C = 0.5 implying higher aromaticity. A decrease of N/C was also observed (Fig. 1C). These structures are related to
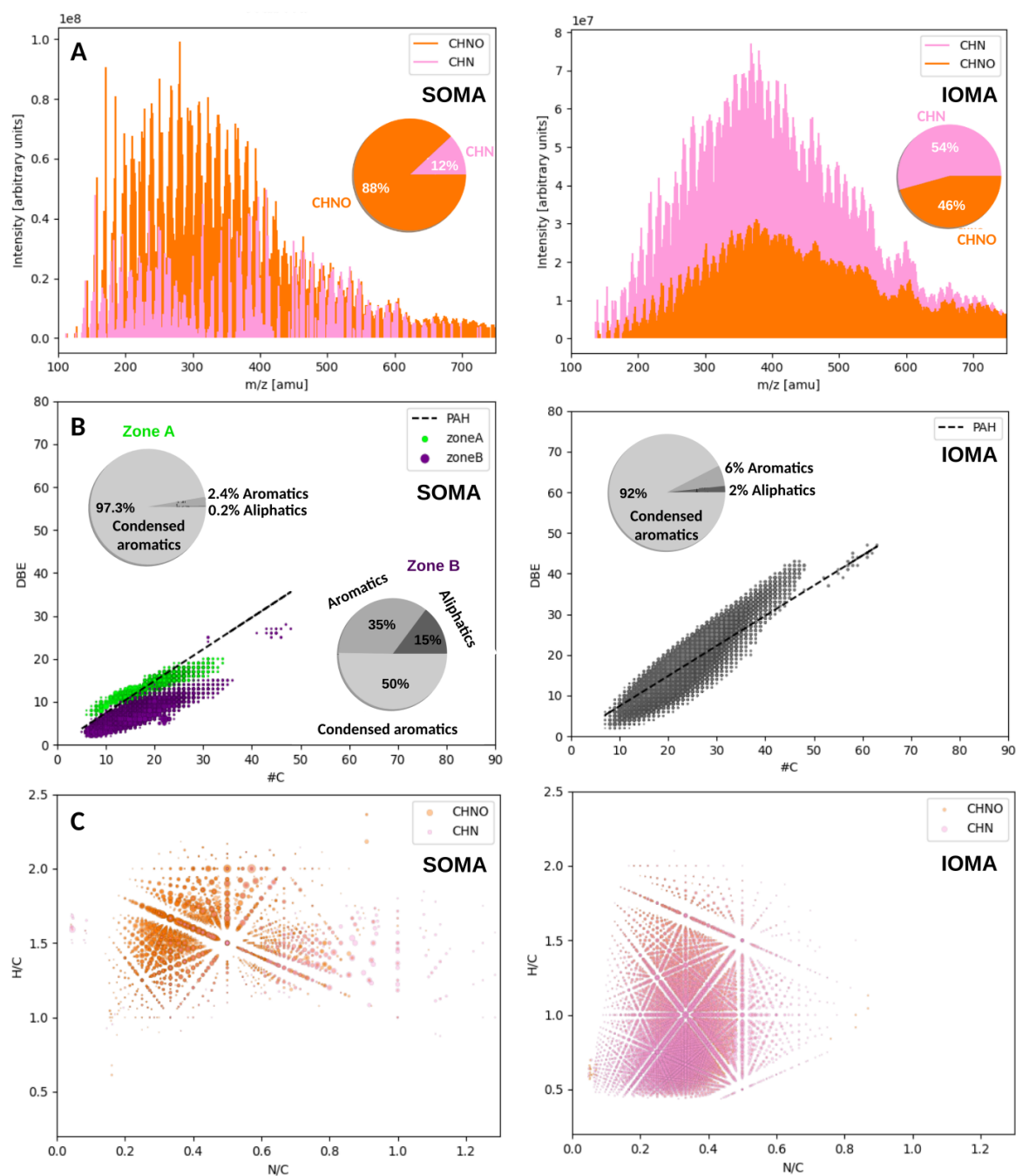
Fig. 1. SOMA versus IOMA. (*A*) Laser desorption ionization FT-ICR mass spectra of analogues of soluble (SOMA, 3756 attributions) and insoluble (IOMA, 9738 attributions) organic matter. Pie charts display the repartition of molecular groups observed (CHNO, CHN) in SOMA and IOMA. (*B*) Representations of double-bond equivalent (DBE) versus the number of carbon (#C) for each molecular formula identified in SOMA and IOMA, with the dotted line indicating the PAH trend. Also displayed are the two different zones of the SOMA (Zone A in green and Zone B in purple). X_C pie chart of SOMA ($m = 0.5$) and IOMA ($m = 0.75$) data are also reported showing attribution repartitions between aliphatic, aromatic and condensed aromatic structures. *m* corresponds to the proportion of O atoms included in double bonds. (*C*) Van Krevelen diagrams H/C versus N/C for SOMA and IOMA.

aliphatic hydrocarbons with various unsaturation impoverished in O (H/C > 1) up to condensed aromatic structures including N in the molecular backbone (H/C < 1), possibly cross-linked with aliphatics. The two zones observed for the SOMA are not present in IOMA (Fig. 1B). Only one distribution is observed, which is depleted in O (Fig. B.1) ranging from zero to three O per attribution with a maximum of attributions presenting one O and an average of 0.6 (Fig. B.2). Attributions are contrariwise rich in N (Fig. B.2) ranging from 2 to 18 N per attribution, with

a maximum at 18 and an average of 8. The average number of C is 25, with an H average of 24, confirming a higher aromaticity of structures compared to SOMA.

2.2. The SOMA/IOMA transition

UV irradiation at 300 K thus induces aromatization of the SOMA and a decrease of its O and N contents leading to an insoluble fraction, which is the IOMA (de Marcellus et al. 2017).
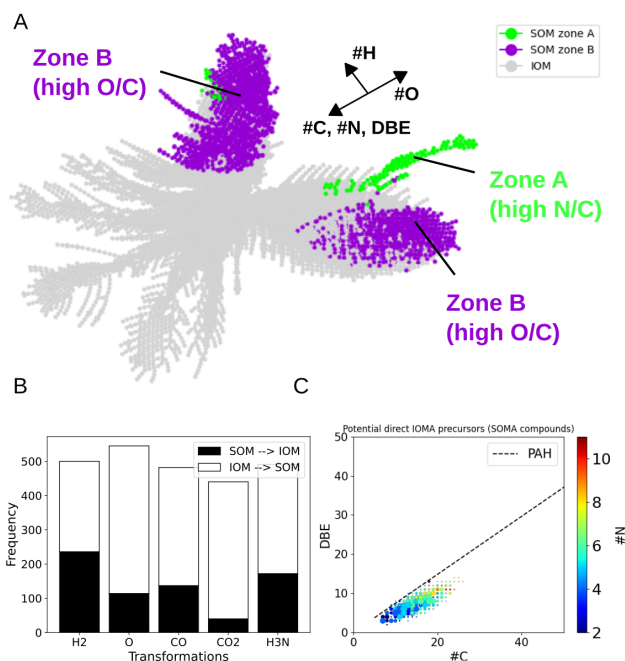
Fig. 2. Molecular network identifying possible connection between SOMA and IOMA. (*A*) One component that represents 70% of SOMA–IOMA attributions displays a connection between SOMA and IOMA. The gray nodes represent the IOMA attributions. (*B*) Frequencies related to edges H_2, O, CO, CO_2, and NH_3 are reported and set as SOMA-to-IOMA or IOMA-to-SOMA transitions. (*C*) SOMA attributions that are directly connected to IOMA ones were extracted and represented as DBE versus #C. These compounds can be considered as direct IOMA precursors.

Next to this IOMA, the remaining soluble fraction of the irradiated SOMA has the mark of this irradiation process. Indeed, its analysis with electrospray ionization showed that some molecules bearing high O/H and O/C disappeared once the SOMA was processed, suggesting a decarboxylation process (Gautier et al. 2020). This trend was confirmed by infrared spectra comparison that indeed present a decrease of vibrators corresponding to COOR chemical functions (Gautier et al. 2020). A gradation in the process of aromatization may occur across the 0.1 μm of irradiated SOMA. To identify these possible SOMA–IOMA transitions, a new representation was developed based on the present LDI analyses using a molecular network illustrating the SOMA–IOMA transition (Fig. 2A). The molecular network was generated by mass difference matching of molecular formulas (nodes in the network) with a set of in-silico transformations that represent potential chemical reactions of H_2, O, CO_2, CO, and NH_3 (Ruf & Danger 2022), induced by the UV processing (edges in the network; Gautier et al. 2020). This data processing should allow us to identify a possible molecular connection between SOMA and IOMA. These connections could then highlight possible precursors transformed during the SOMA irradiation and leading to the first IOMA molecules. One component of the obtained network, representing 70% of all detected SOMA–IOMA molecular formulas, connects SOMA to IOMA attributions. SOMA molecules are grouped on the outer part and aligned by #H, #C, and DBE gradients (Figs. 2 and B.5). SOMA–IOMA transitions are displayed in three zones. Two are related to Zone B of SOMA (enriched in O, Fig. 1B). These two SOMA zones are different in their transformations' fingerprints and element maps (e.g., #H, #C, #N, #O, and *m/z*). Next, a third zone is related
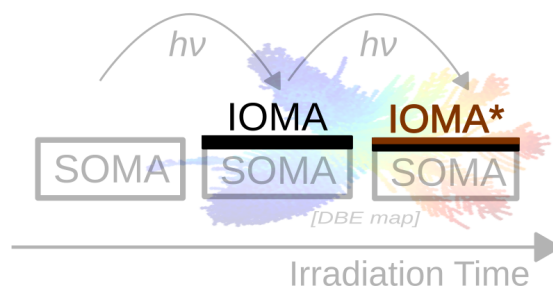
Fig. 3. Possible evolution process leading to the formation of IOMA from SOMA. The upper 0.1 μm layer of the SOMA are UV irradiated, leading to the formation of the first IOMA molecules (dark). Once formed, these IOMA first-generation molecules are UV irradiated, leading to an evolved generation of IOMA (brown). This evolution is visible in the gradient of #C, #N, and DBE of elementary maps (Fig. B.5).

to Zone A (enriched in N). Connections (Fig. 2B) are driven equally by H_2 edges (balanced in addition/subtraction), followed by similar amounts of CO, O, and NH_3 edges. CO, O, and NH_3 are preferentially subtracted (IOMA -> SOMA, see histograms in Fig. 2B) confirming previous observations. SOMA transition nodes (Fig. 2C, molecules that are directly connected to IOMA molecules) show a wide range in #C, from 5 to 27, low #O counts (maximum of #O = 3), and high #N (maximum of #N = 11).

In this network, it is interesting to note that SOMA/IOMA connections are only located in two lobes. Regarding elementary maps (Fig. B.5), from SOMA–IOMA lobes to IOMA alone (gray, Fig. 2A), an increase in #DBE, #C, and #N is observed, while #O decreases. This gradient seems to follow an evolutionary process related to UV irradiation of the material. It would start from SOMA molecules that evolve to form the first IOMA molecules, decreasing the #O counts while starting to increase the DBE as well as #C and #N counts. This process occurred on the first 0.1 μm of UV penetration depth in SOMA. While the first IOMA molecules directly formed from SOMA, they can be further irradiated leading to an evolution of the IOMA itself (gradient observed in elementary maps). Therefore, two IOMA generations can be formed, one of which is directly connected to the SOMA, as observed in the two lobes, and another one that is linked to the degradation of the first IOMA generation itself under the UV processing (Fig. 3).

3. Discussion

3.1. Analogs versus Paris meteorite

We propose that a fraction of the IOM of meteorites can be generated by the processing, under radiations (UV, electrons and/or ions), of a soluble ice residue (Danger et al. 2021) at the surface of grains before the parent body accretion. In this section, the IOM of Paris is compared to the IOMA (Fig. 4). The comparison of DBE versus #C representations show that attributions are aligned along the same slope, which is the PAH line. Furthermore, as described in Danger et al. (2020), two zones were present for the Paris IOM. Even if these two zones are less visible for IOMA, they are still present. These observations imply that the Paris IOM and IOMA share similar aromaticities. This is confirmed by the X_C factor showing a same percentage of condensed aromatic, aromatics and aliphatics (Fig. 4A). Both Paris IOM and IOMA are depleted in O (Fig. 4B). Furthermore, both also have a higher number of carbon atoms per molecule than for hydrogen, confirming the high aromaticity of these materials. The comparison of VK H/C versus O/C also
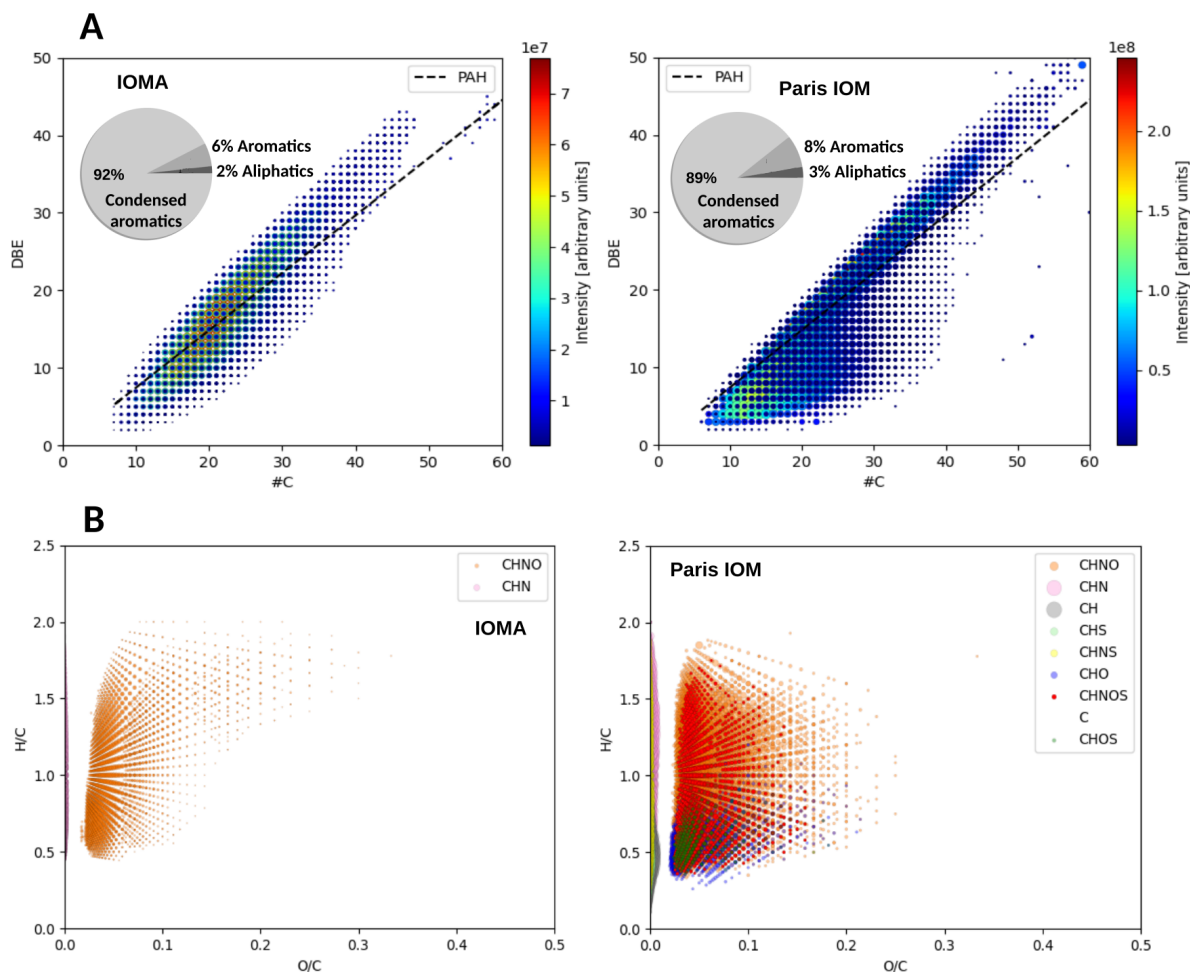
Fig. 4. IOMA versus IOM of Paris. (*A*) Representations of DBE versus the number of carbon (#C) for IOMA and IOM, with X_C pie charts showing attribution repartitions between aliphatic, aromatic, and condensed aromatic structures. (*B*) Van Krevelen H/C versus O/C for attributions identified in IOMA and IOM of Paris meteorite. For the Paris meteorite, data were reproduced from Danger et al. (2020).

shows interesting similarities in the attribution distribution in the VK space (Fig. 4B). Attributions are aligned to H/C = 1, with H/C ranging from 0.5 to 2 with a maximum of O/C around 0.2. Therefore, regarding aromaticity and O content, IOMA and the Paris IOM present similarities. However, a higher amount of N is present in the IOMA compared to the Paris IOM (Fig. B.4). This is coherent with the higher N content observed in SOMA compared to the meteorite SOM (Danger et al. 2016). Indeed, the SOMA enriched in N, the IOMA, which originates from it, keeps this N enrichment, even if a decrease in N is observed from SOMA to IOMA due to the UV processing. It should also be noted that in our analog formation experiment, no sulfur is yet incorporated. S is very abundant in the SOM and IOM of meteorites and certainly plays an important role in the chemistry that led to these organic materials. In particular, it may impact the redox chemistry in the parent bodies of the meteorites if aqueous alteration has occurred. Therefore, the next step is to incorporate this heteroatom into our experiments to test its impact on the chemical reactivity leading to our SOMAs and IOMAs, as we begin to experiment by bombarding the ices as well as the SOMAs with sulfur ions (Ruf et al. 2021, 2019a).

Finally, since the molecular network presented in Fig. 2 provides an insight into the SOMA–IOMA transitions generated by UV processing, it was applied to the SOM–IOM of the Paris meteorite in order to identify if some SOM–IOM transitions related to the same process could be isolated. The Paris

SOM was firstly analyzed with LDI-FTICR-MS. The SOM–IOM molecular network was then obtained (Fig. B.6) using the same edges (H_2, CO, O, CO_2, NH_3) as SOMA–IOMA. The obtained molecular network is clearly different. This implies that the putative evolution of SOM into IOM would be much more complex than only through UV photochemistry. This may be the consequence of parent-body evolution. Even if the Paris meteorite is among the less altered, secondary processings have occurred in the parent body and have induced the modification of the accreted OM (Vinogradoff et al. 2017). Furthermore, numerous pathways could have led to IOM and SOM formation in the meteorite parent bodies (Remusat et al. 2010; Vinogradoff et al. 2017). However, it is interesting to note that two components linking SOM to IOM have been identified (Figs. B.6 and B.7), implying that a possible connection could exist as observed in our experiments, since the same edges are used. The number of connections is much lower than the one observed for SOMA–IOMA, but this could suggest that a part of SOM and IOM of the Paris meteorite is related through radiation processes and that the organic content of the Paris meteorite kept this trace.

3.2. Dense molecular ices as a source of chondritic SOM and IOM in meteorites

Numerous experiments have shown that dense molecular ice analogues can generate an important molecular diversity during

simulated solar nebula evolution. Organics formed are soluble in polar solvent, and their molecular diversity can be related to the SOM of meteorites that is the last step of evolution in the interplanetary objects of the Solar System. However, SOMA is significantly different in its molecular content than the Paris SOM. This can be explained because SOMA directly originates from ices and thus has not undergone parent body evolution, which opposite to the case of the organic molecules contained in chondrites. That is why SOMA has to be considered as a possible analogue of the pre-accretionnal organic matter that was then incorporated in chondrite parent bodies. This hypothesis is strengthened when a SOMA is altered in conditions simulating a secondary aqueous alteration at 150 °C and six bars, commensurable to asteroid conditions (Danger et al. 2021). It leads to the formation of molecules sharing numerous similarities with chondrite SOM. Hence, the content of nitrogen is depleted after 100 days of reaction. Consequently, dense molecular cloud ices could be considered as precursors of a fraction of the SOM observed in chondritic meteorites. One may question if it is the same for the insoluble organic fraction of chondritic meteorites.

In addition to a soluble fraction, dense molecular ices can also lead to the formation of insoluble organic material if subjected to intense UV irradiation. The material is formed by the evolution of the soluble fraction at the surface of evolved ice grains. It could then be accreted with silicate and metal grains to form parent bodies of meteorites. It must be noted that formation of IOM from soluble compounds during alteration under asteroidal conditions is hampered by the presence of clay minerals (Viennet et al. 2022; Vinogradoff et al. 2020). IOMA and IOM share several molecular characteristics: aromaticity, molecular diversity, and O content, even if some differences remain, such as a higher amount of N in IOMA. However, as shown for SOMA, IOMA may also undergo secondary alteration once incorporated in the meteorite parent bodies. Some experiments have indeed shown that the processing of organic content of meteorites released an important fraction of nitrogen (Pizzarello et al. 2011). If the same effect as the one observed on SOMA occurs, a possible evolution of IOMA could occur and bring it closer to the IOM molecular content.

Experimental simulations thus give important clues on the role that dense molecular cloud ices play in the origin of the organic matter available in the Solar System. During their evolution through various types of irradiation (VUV, X-Rays, Cosmic Rays and/or electrons), radical and thermal chemistry led to their molecular evolution and resulted in an increased molecular diversity. The obtained organic compounds could then be modified by solar radiative environments and thermal processes in the mid-plane of the protosolar nebula, toward an insoluble organic material. After accretion on the parent bodies, these organic materials can then undergo secondary processes, notably through aqueous alteration, which induces the aromatization and oxidation of the accreted organic components (Kebukawa et al. 2020; Vinogradoff et al. 2018). Consequently, next to the gas phase, the solid phase (e.g. particularly dense molecular ices) has to be taken into account as a source of organic matter of the Solar System objects.

References

Brearley, A. J. 2006, Meteorites and the Early Solar System II, 943, 587

Cho, Y., Jin, J. M., Witt, M., et al. 2013, Energy Fuels, 27, 1830

Cody, G., Alexander, C. O., & Tera, F. 2002, Geochim. Cosmochim. Acta, 66, 1851

Danger, G., Orthous-Daunay, F.-R., de Marcellus, P., et al. 2013, Geochim. Cosmochim. Acta, 118, 184

Danger, G., Fresneau, A., Abou Mrad, N., et al. 2016, Geochim. Cosmochim. Acta, 189, 184

Danger, G., Ruf, A., Maillard, J., et al. 2020, Planet. Sci. J., 1, 55

Danger, G., Vinogradoff, V., Matzka, M., et al. 2021, Nat. Commun., 12, 1

de Marcellus, P., Fresneau, A., Brunetto, R., et al. 2017, MNRAS, 464, 114

Fresneau, A., Abou Mrad, N., d'Hendecourt, L. L., et al. 2017, ApJ, 837, 168

Gardinier, A., Derenne, S., Robert, F., et al. 2000, Earth Planet. Sci. Lett., 184, 9

Gautier, T., Danger, G., Mousis, O., et al. 2020, Earth Planet. Sci. Lett., 531, 116011

Hagberg, A., Swart, P., & S Chult, D. 2008, Exploring network structure, dynamics, and function using NetworkX, Tech. rep., Los Alamos National Lab. (LANL), Los Alamos, NM, USA

Kebukawa, Y., Nakashima, S., Mita, H., Muramatsu, Y., & Kobayashi, K. 2020, Icarus, 347, 113827

Le Guillou, C., & Brearley, A. 2014, Geoch. Cosmoch. Acta, 131, 344

Le Guillou, C., Bernard, S., Brearley, A. J., & Remusat, L. 2014, Geochim. Cosmochim. Acta, 131, 368

Maillard, J., Carrasco, N., Schmitz-Afonso, I., Gautier, T., & Afonso, C. 2018, Earth Planet. Sci. Lett., 495, 185

Marshall, J. W., Schmitt-Kopplin, P., Schuetz, N., et al. 2018, Food Chem., 242, 316

Pearson, V., Sephton, M., Franchi, I., Gibson, J., & Gilmour, I. 2006, Meteor. Planet. Sci., 41, 1899

Pizzarello, S. 2007, Origins Life Evol. Biospheres, 37, 341

Pizzarello, S., Williams, L. B., Lehman, J., Holland, G. P., & Yarger, J. L. 2011, Proc. Natl. Acad. Sci. U.S.A., 108, 4303

Remusat, L., Derenne, S., & Robert, F. 2005a, Geochim. Cosmochim. Acta, 69, 4377

Remusat, L., Derenne, S., Robert, F., & Knicker, H. 2005b, Geochim. Cosmochim. Acta, 69, 3919

Remusat, L., Guan, Y., Wang, Y., & Eiler, J. 2010, ApJ, 713, 1048

Ruf, A. & Danger, G. 2022, Anl. Chem., 94, 14135

Ruf, A., d'Hendecourt, L. L., & Schmitt-Kopplin, P. 2018, Life, 8, 18

Ruf, A., Bouquet, A., Boduch, P., et al. 2019a, ApJ, 885, L40

Ruf, A., Poinot, P., Geffroy, C., Le Sergeant d'Hendecourt, L., & Danger, G. 2019b, Life, 9, 35

Ruf, A., Bouquet, A., Schmitt-Kopplin, P., et al. 2021, A&A, 655, A74

Schmitt-Kopplin, P., Gabelica, Z., Gougeon, R. D., et al. 2010, Proc. Natl. Acad. Sci. U.S.A., 107, 2763

Schmitt-Kopplin, P., Harir, M., Kanawati, B., et al. 2012, Meteorites 2012, 79

Tziotis, D., Hertkorn, N., & Schmitt-Kopplin, P. 2011, Eur. J. Mass Spectrom., 17, 415

Van Rossum, G., & Drake Jr, F. L. 1995, Python tutorial, 620 (Centrum voor Wiskunde en Informatica Amsterdam, The Netherlands)

Viennet, J.-C., Le Guillou, C., Remusat, L., et al. 2022, Geochim. Cosmochim. Acta, 318, 352

Vinogradoff, V., Le Guillou, C., Bernard, S., et al. 2017, Geochim. Cosmochim. Acta, 212, 234

Vinogradoff, V., Bernard, S., Le Guillou, C., & Remusat, L. 2018, Icarus, 305, 358

Vinogradoff, V., Le Guillou, C., Bernard, S., et al. 2020, Geochim. Cosmochim. Acta, 269, 150

Yabuta, H., Naraoka, H., Sakanishi, K., & Kawashima, H. 2005, Meteor. Planet. Sci., 40, 779

Yassine, M. M., Harir, M., Dabek-Zlotorzynska, E., & Schmitt-Kopplin, P. 2014, Rapid Commun. Mass Spectrom., 28, 2445

Appendix A: Methods

A.1. SOMA and IOMA formation

For the formation of SOMA, a gas mixture of $H_2O:CH_3OH:NH_3$ (2:1:1) was first deposited onto an inert MgF_2 window at 77 K at 10^{-8} mbar, forming an astrophysical ice analogue. 77 K simulates the position of an icy grain on the edge of a protoplanetary disk where it can receive a sufficient dose of Lyman α photons. Irradiation of deposited gas-ice was performed simultaneously over 72 h at 77 K using microwave-generated H_2 plasma with a constant molecular hydrogen flow providing vacuum UV photons (at Lyman α (121 nm) with a flux of 2 x 10^{14} photons cm^{-2} s^{-1}). Ice composition and irradiation were monitored using a Bruker Vector 22 infrared spectrometer (400-4000 cm^{-1}, 20 scans per spectrum with a 1 cm^{-1} resolution). After 72 h of deposition and irradiation, the UV dose in the experiments presented here was 5.2 x 10^{19} photons cm^{-2}. This roughly corresponds to a grain submitted to 1.7 x 10^6 photons cm^{-2} s^{-1} during a lifetime of the solar nebula of 1 x 10^6 yr. The photo-processed ice was then slowly warmed up to 300 K with 0.1 K per minute. A SOMA sample of approximately 100 µg, entirely soluble in polar solvent, remained in the MgF_2 window. This SOMA was then kept at 300 K under 10^{-7} mbar. Two SOMA samples were formed following this process. One was then irradiated over 72 h at Lyman α leading to the formation of an insoluble fraction in any solvent at the top of the SOMA sample, which is the insoluble organic matter analog (IOMA). Both samples were then kept in their MgF_2 windows at 5°C and 10^{-6} mbar up to their analyses.

A.2. Paris SOM extraction

A 10 mg Paris CM chondrite was first washed with LCMS-grade methanol (Fluka) to remove surface contamination; this washing fluid was discarded. After that, it was crushed and ground in an agate mortar with an agate pestle for 60 sec under 400 µl LCMS-grade methanol. The solutions were centrifuged at 16000 rpm (rounds per minute) for 3 minutes. The obtained supernatant was directly used for ultra-high resolution mass spectrometry as described in the FT-ICR-MS analysis section.

A.3. FT-ICR-MS analyses

All analyses were performed in Rouen, France, on a FT-ICR SolariX XR mass spectrometer equipped with a 12 T superconducting magnet (Buker Daltonics, Germany). The FT-ICR-MS is also equipped with a laser desorption ionization source (laser NdYAG x 3) allowing the analysis of both liquid and solid samples. Samples were directly analyzed on their MgF_2 windows. It is important to note that since the IOMA was formed on the top of the SOMA sample and that the UV irradiation only penetrates approximately 0.1 µm in the SOMA, it remains SOMA below the IOMA. Therefore, for the IOMA analyses, the penetration depth of the laser during the LDI step was monitored in order to not ionize the SOMA that is below the IOMA crust. Spectra were recorded in broadband mode with a mass range set between m/z 122 and m/z 1200. Free induction decays (FID) were digitized using four million points. 500 FID were accumulated for each spectrum in positive mode. The following instrumental parameters were implemented: plate offset 100 V, deflector plate 200 V, laser shots 70, laser shots frequency 2000 Hz, funnel 1 at 150 V, and skimmer 1 at 25 V. Laser power was optimized following a previous published procedure (Marshall et al. 2018). For IOMA, laser power was set at 28%. For SOMA, laser power was raised to 30%. It should be noted that the laser power is significantly higher than previously published results because the thickness of the MgF_2 is 1 millimeter and causes a defocusing of the laser. This means that for the same laser power, the fluence delivered is much lower. In addition, this thickness induced a nonideal reproducibility between analyses. To compensate that, analyses were recorded in triplicate for each sample. Triplicates were then merged together, and only molecular formulas common to all triplicates were kept ensuring relevant results. The same protocol was applied to analyze the Paris SOM sample.

A.4. MS data analysis

Mass spectra were exported to peak lists at a signal-to-noise ratio of three. Mass resolving power was 400,000 at m/z = 400 with a mass accuracy of <0.5 ppm, enabling the separate detection of isobars differing by less than the mass of an electron. Practically, this approach enables a direct assignment of molecular compositions with C, H, N, O, and S atoms (and isotopologues in natural abundance) for each individual exact mass (m/z value). Molecular formulas were assigned from exact m/z values by mass difference network analysis for each peak in batch mode by an in-house software tool Tziotis et al. (2011) and validated via the senior-rule approach/cyclomatic number. For each data sample, all attributions in common with blanks were deleted from the data set. The double-bound equivalent was obtained from the following general formula: DBE = n(C) - n(H)/2 + n(N)/2 + 1. Calculation of X_C. The aromaticity equivalent X_C was calculated according to the following formula (Yassine et al. 2014): $X_C = ((2*n(C) + n(N) - n(H) - 2*m*n(O))/(DBE - m*n(O))) + 1$, where m corresponds to an estimate of the oxygen fraction linked to carbon by double bonds: m=0.75 for IOMA and m=0.5 for SOMA. Chemical classes, aliphatics, aromatics, and condensed aromatics were defined accordingly: aliphatics $0 < X_C < 2.5$, aromatics (one aromatic ring, like benzene) $2.5 < X_C < 2.7$, and condensed aromatics (more aromatic rings like in PAH) $2.7 < X_C$. From these X_C values, the degree of aromaticity will be estimated based on the distribution between condensed aromatics, aromatics, and aliphatics. The PAH line shown in Figs. 1, 2, 4, B.3, and B.6 is based on a linear fit of DBE and #C for 73 PAH compounds from polycyclic aromatic hydrocarbons (evaluation of sources and effects; [1] equation of linear regression: y = 0.74x + 0.054). The fullerene line in Fig. B.3 is based on a linear fit of 14 fullerene compounds from C_{20} to C_{90}.

A.5. Molecular network generation and analysis

Theoretical ion masses of prior assigned molecular formulas were used for network generation, as performed via Python (Van Rossum & Drake Jr 1995). Theoretical ion masses (nodes in the network) were connected by edges (transformations) if their mass differences matched with the theoretical mass differences of the transformations that represent potential chemical reactions (e.g., for the "minimal set" of transformations, used as a basis for this study): ΔH_2, ΔO, ΔCO, ΔNH_3, with $\Delta H_2 = 2.01565$ u, $\Delta O = 15.994915$ u, $\Delta CO = 27.994915$ u, and $\Delta NH_3 = 17.026549$ u, with u being the unified atomic mass unit. Molecular network analysis was performed via Python (Van Rossum & Drake Jr 1995), and, specifically, networkX (Hagberg et al. 2008) was used for graph computations and network layouts (graphviz layout). Networks allow us to visualize and spatially cluster the complex chemical spaces of SOMA

---

[1] https://www.ncbi.nlm.nih.gov/books/NBK217760/

and IOMA based on the molecules' interactions. Element maps represent molecular cartography and further organize the complex molecular network. All computations were performed on a stand-alone computer. Molecular networks were generaraed and analyzed via the method mol2net (https://zenodo.org/record/7025094; Ruf & Danger 2022).

Appendix B: Supporting figures
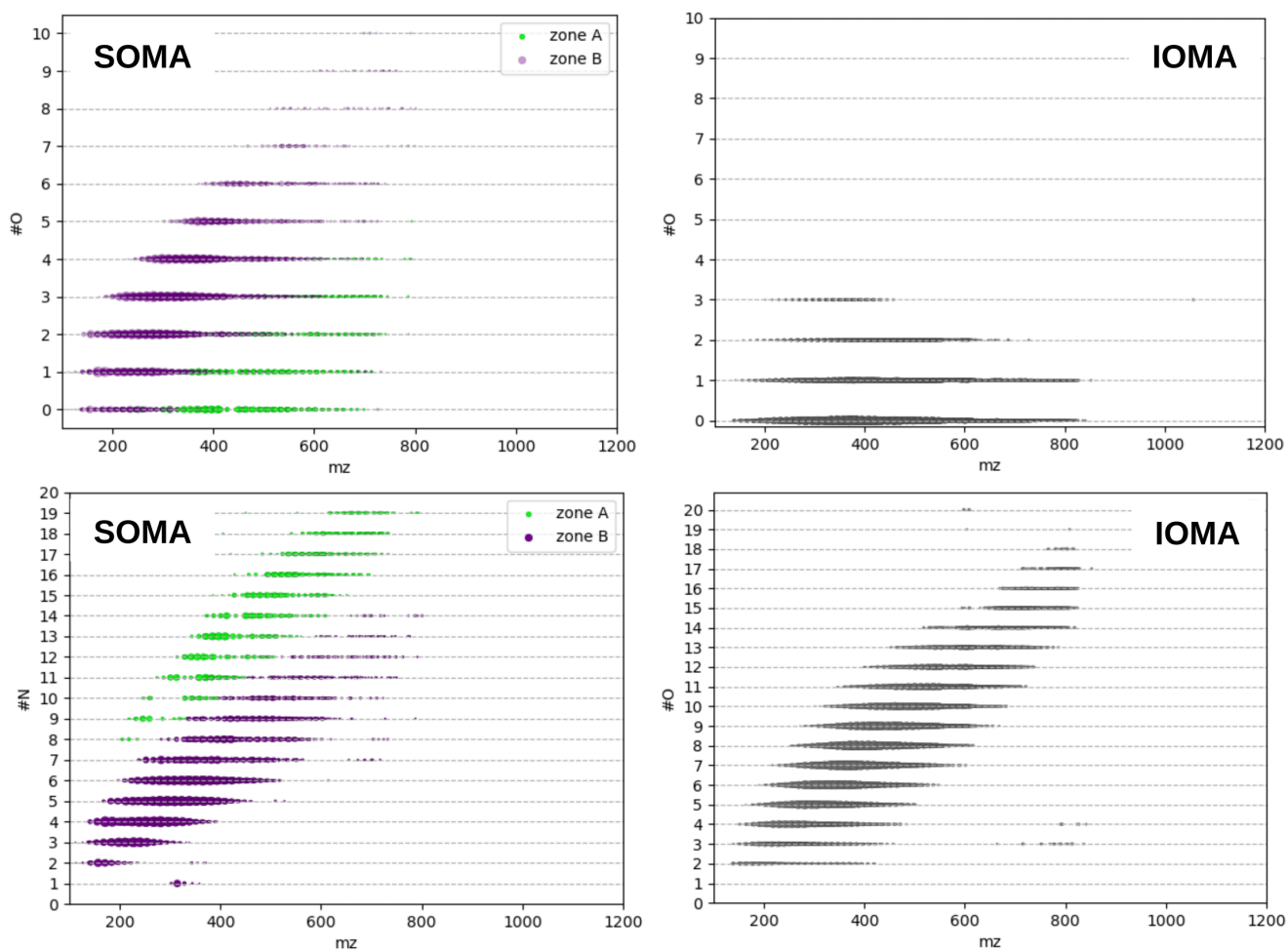
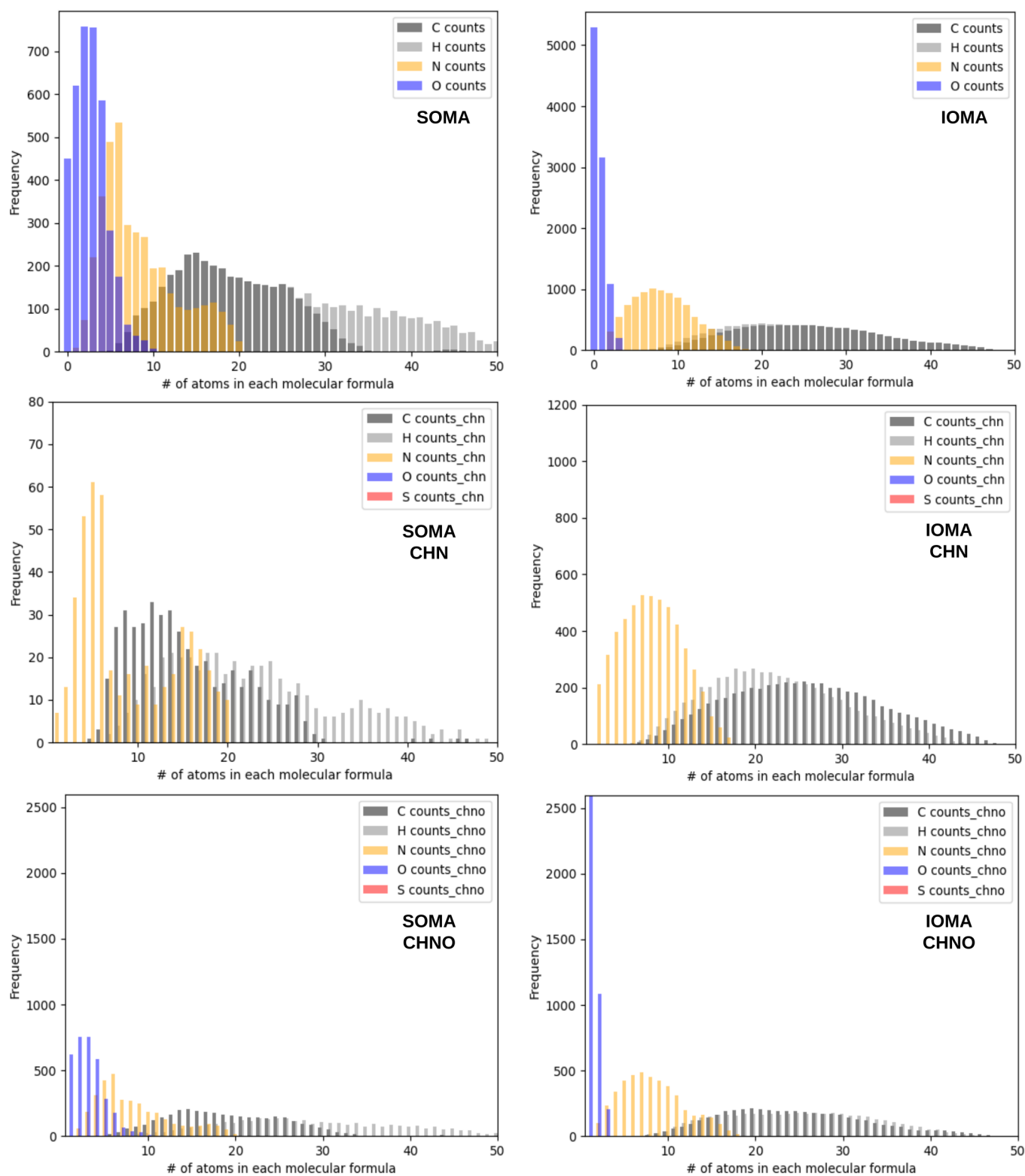**Fig. B.1.** Evolution of O or N elements as a function of m/z for SOMA or IOMA for all attributions or for CHNO or CHN groups only.

Fig. B.2. Frequencies of atoms in each molecular formula for all attributions, CHNO, or CHN (groups for SOMA and IOMA).
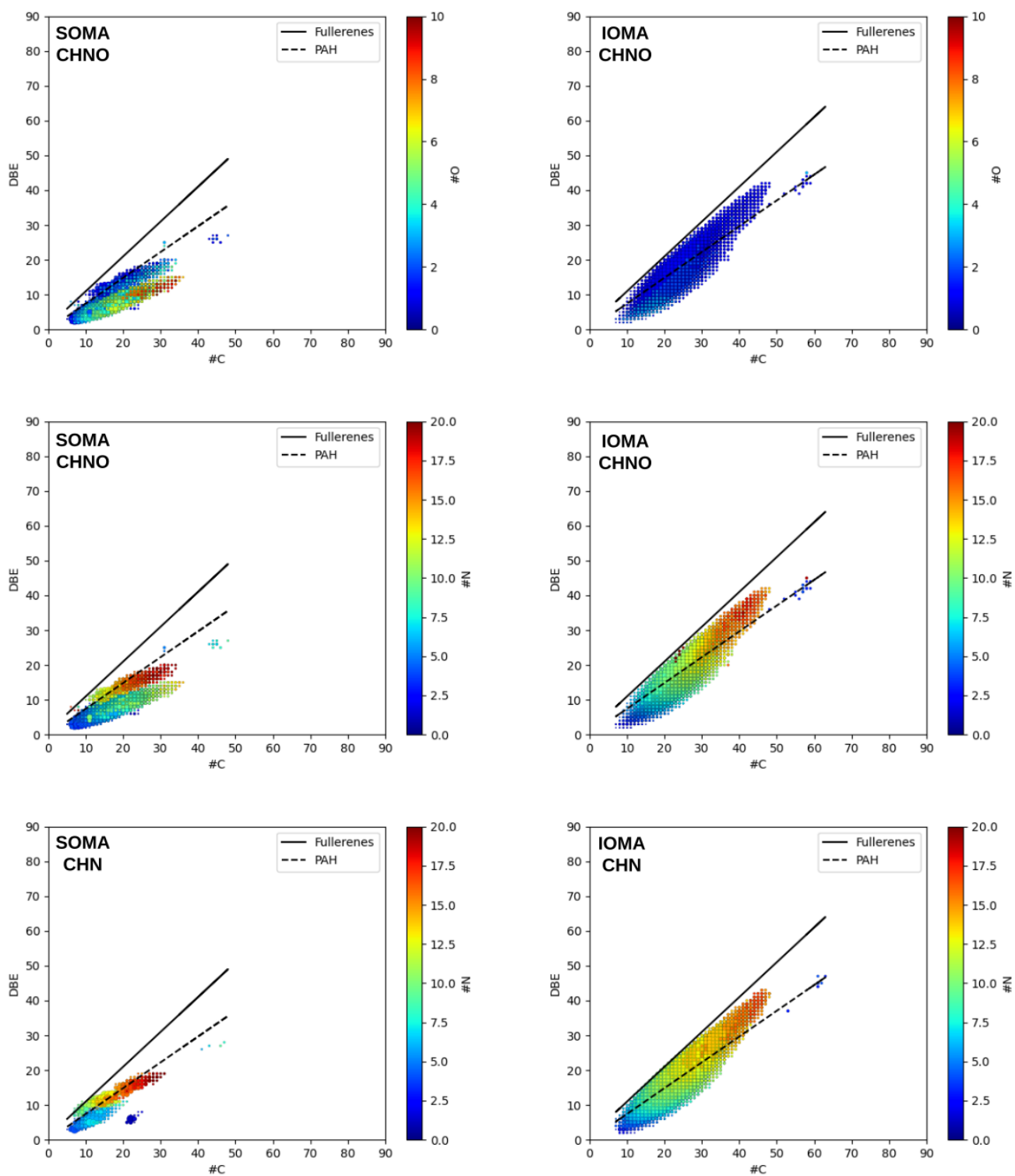
Fig. B.3. Representations of double-bond equivalent (DBE) versus the number of carbon (#C) for the CHNO or CHN formula identified in IOMA and SOMA, with the dotted line indicating the PAH trend. Also displayed are the color map proportional to the number of O or N atoms in formulas.
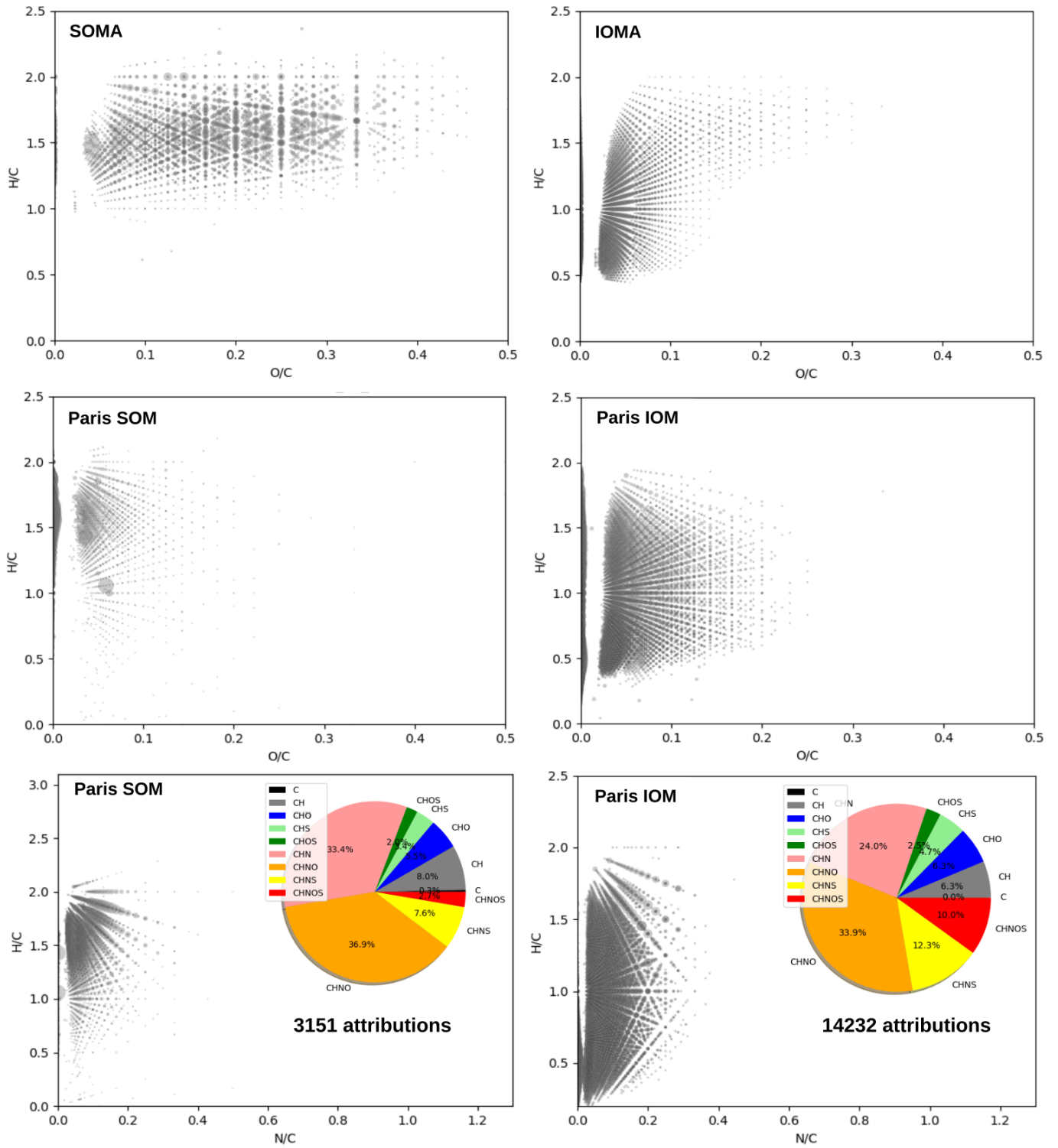
Fig. B.4. Van Krevelen diagrams with H/C versus N/C for O/C or IOMA, SOMA, SOM, or IOM of Paris meteorite.
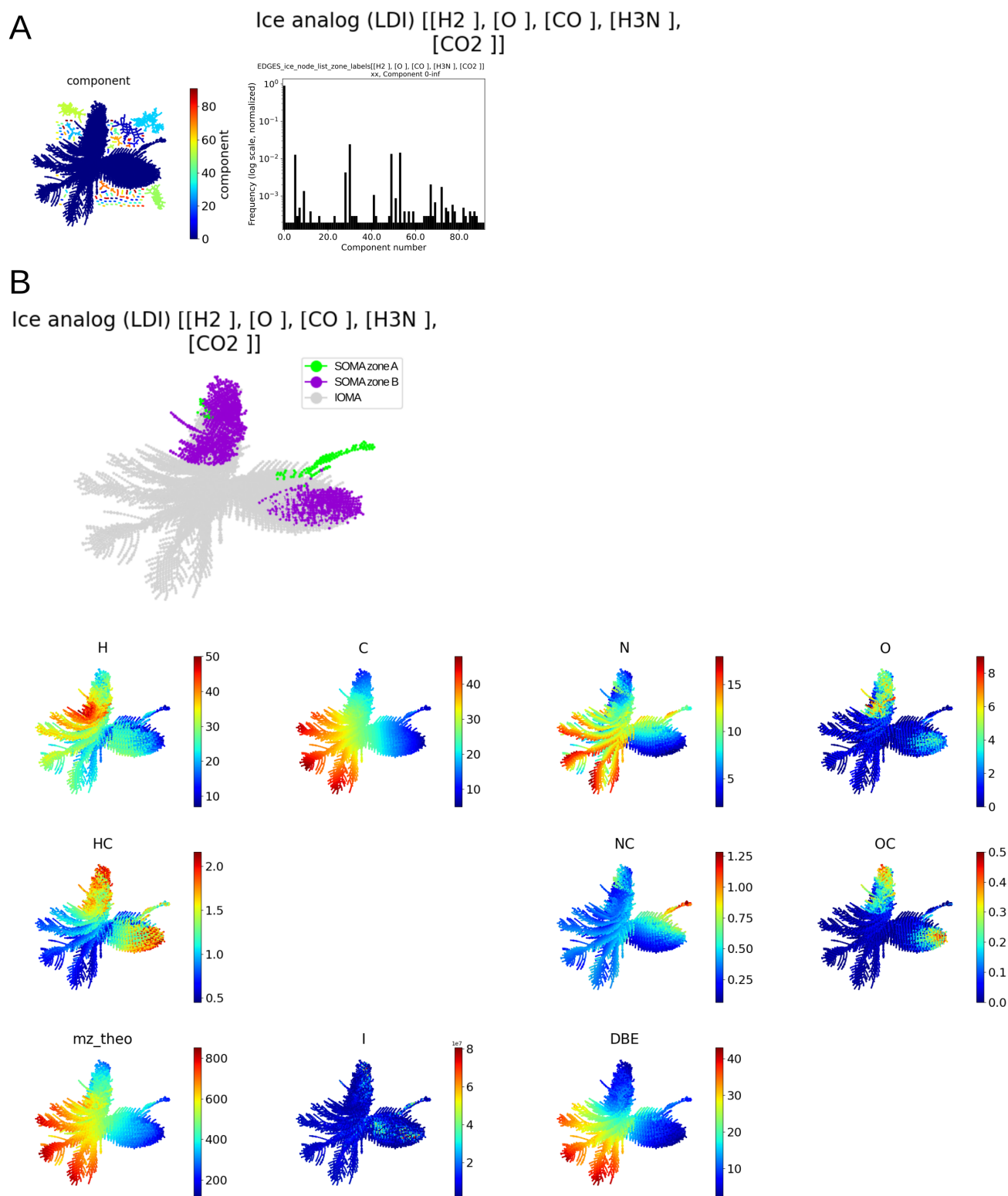
Fig. B.5. Information related to the molecular network of analogs. (A) All graph components of analog network. (B) Element maps of the analog network.
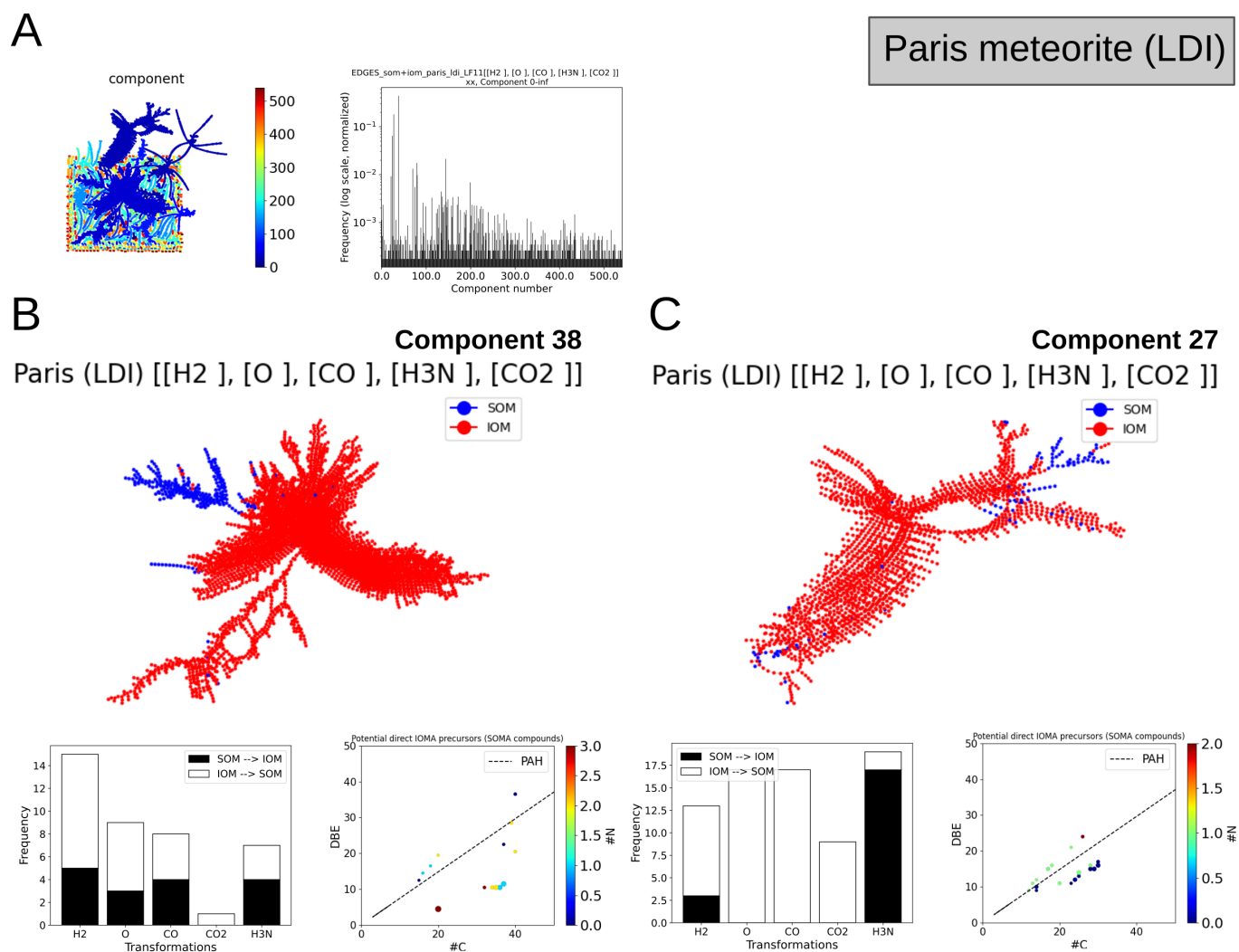
Fig. B.6. Molecular network related to SOM–IOM of Paris. (A) All graph components of Paris meteorite network. (B) Two SOM–IOM transition graph components, number 38 and number 27, have been identified and their characteristics are represented.
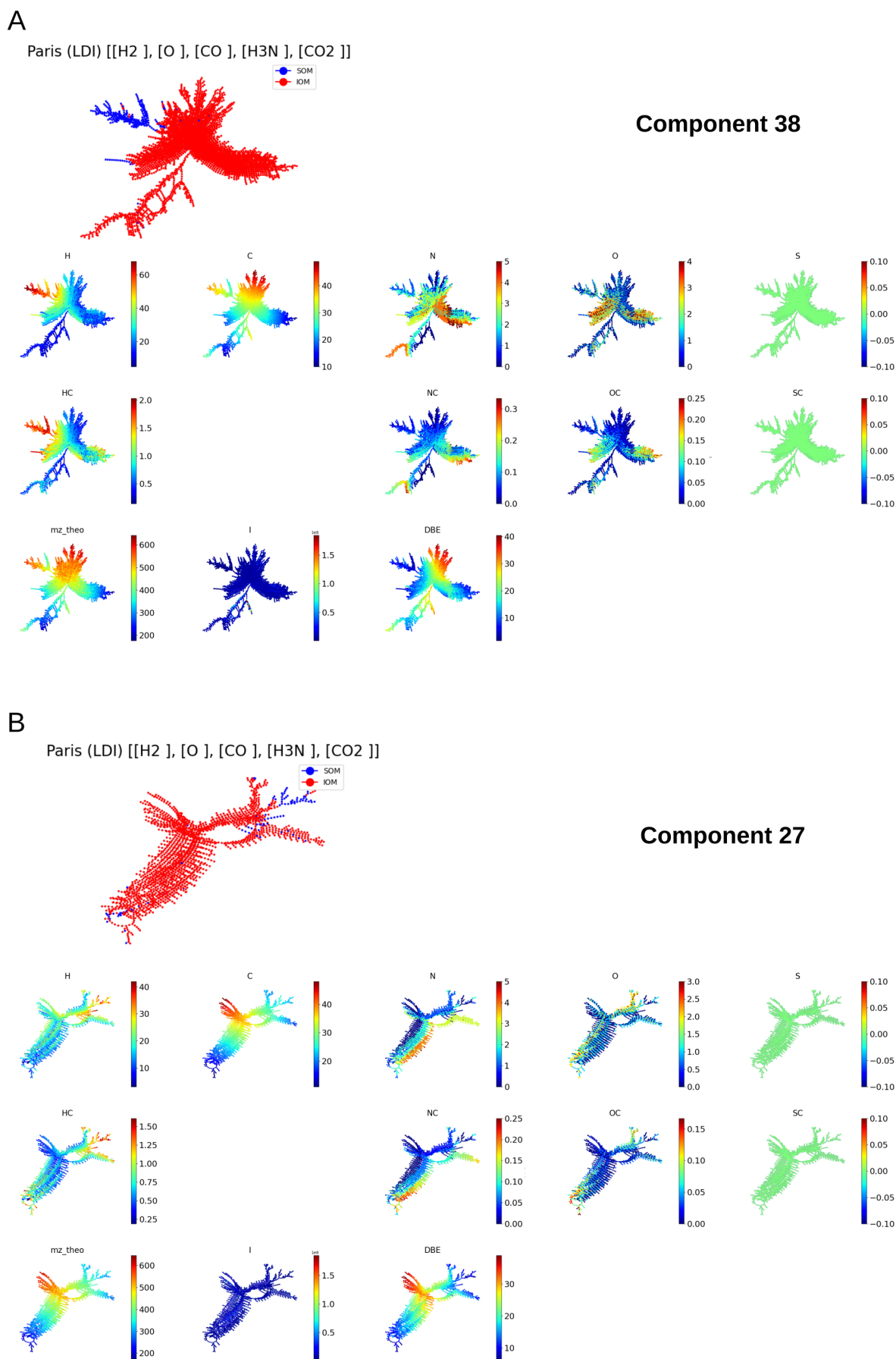
A

Paris (LDI) [[H2], [O], [CO], [H3N], [CO2]]

Component 38

B

Paris (LDI) [[H2], [O], [CO], [H3N], [CO2]]

Component 27

Fig. B.7. Element maps of SOM–IOM transition graph components number 38 (A) and number 27 (B) for Paris meteorite network.